Effect of Nitrogen Alloying on the Microstructure and Abrasive Wear of Stainless Steels

J.A. Hawk, J.W. Simmons, and J.C. Rawers

Alloying stainless steels with nitrogen has distinct advantages. Nitrogen is a strong austenite stabilizer and a potent solid-solution strengthener, and nitrogen has greater solubility than carbon in iron. This study investigates the relationship among nitrogen concentration, precipitate microstructure, and abrasive wear using two high-nitrogen stainless steel alloys: Fe-19Cr-5Mn-5Ni-3Mo (SS1) and Fe-16Cr-7Mn-5Ni (SS2). Alloy SS1 contained 0.7 wt% N and was solution annealed at 1150 °C, thereby dissolving the nitrogen interstitially in the austenite. Subsequent aging, or cold work and aging, at 900 °C led to the grain-boundary, cellular, and transgranular precipitation of Cr_2N. Alloy SS2 was remelted in a high-pressure (200 MPa) N_2 atmosphere, leading to a spatial gradient of nitrogen in the alloy in the form of interstitial nitrogen and Cr_2N and CrN precipitates. Nitrogen contents varied from a low of approximately 0.7 wt% at the bottom of the billet to a high of 3.6 wt% at the top. Nitrogen in excess of approximately 0.7 wt% formed increasingly coarser and more numerous Cr_2N and CrN precipitates. The precipitate morphology created in alloy SS1 due to aging, or cold work and aging, had little effect on the abrasive wear of the alloy. However, a decrease in the abrasive wear rate in alloy SS2 was observed to correspond to the increase in number and size of the Cr_2N and CrN precipitates.

Keywords

abrasive wear, chromium nitride, nitrogen stainless steel

1. Introduction

ALLOYING austenitic stainless steels with nitrogen offers several advantages. Nitrogen is a strong austenite stabilizer and solid-solution strengthener, reduces the tendency for martensitic transformation, and improves pitting corrosion resistance (Ref 1, 2). Nitrogen, at levels below 0.4 wt%, has been used as an alloying element in stainless steels for more than 40 years. Initially, the role of nitrogen was primarily as an austenite stabilizer, used to replace nickel, a costly alloy addition. More recently, nitrogen has been used to replace carbon, such as in the AISI 304LN and 316LN grades, in order to produce alloys with strengths similar to carbon steels, but with less susceptibility to sensitization. Currently, nitrogen is used as the primary solid-solution strengthening agent and is very effective in this role.

A major obstacle to alloying with nitrogen is its low solubility in liquid iron: only 0.045 wt% at 1600 °C and atmospheric pressure. However, nitrogen solubility can be significantly enhanced through alloying and/or increasing the N_2 gas pressure above the melt. Additions of chromium and manganese increase nitrogen solubility, whereas nickel reduces solubility. For example, the AISI 200 series and Nitronic (Armco Inc., Middletown, OH) austenitic stainless steels, based on the Fe-Cr-Mn-Ni-N system, were designed for increased nitrogen solubility through alloying. Even with alloying, nitrogen concentrations in conventionally processed Fe-Cr-Mn-Ni stainless steels are still restricted to less than about 0.4 wt%. However, recent developments in high-pressure processing technologies have made it possible to produce high-nitrogen stainless steels with nitrogen levels exceeding 1 wt%. The focus of this research is to investigate the effect of nitrogen additions on the microstructural morphology of Fe-19Cr-5Mn-5Ni-3Mo (SS1) and Fe-16Cr-7Mn-5Ni (SS2) and to assess the wear resistance of the alloys as a consequence of changes in alloy microstructure.

J.A. Hawk, J.W. Simmons, and **J.C. Rawers,** U.S. Bureau of Mines, Albany Research Center, Albany, OR 97321, USA

1.1 *Nitrogen Solubility*

Nitrogen solubility in liquid iron-base alloys generally follows Sievert's law and is proportional to the square root of the N_2 gas pressure over the melt (Ref 3-5), as illustrated in Fig. 1. Higher pressures and/or nitrogen levels cause deviation from Sievert's law, and increases in nitrogen concentrations with pressure occur to a power of less than ½. The effect of alloy additions on nitrogen solubility in iron at 1600 °C, normalized to chromium, is shown in Fig. 2. Elements that have the greatest positive influence on nitrogen solubility in the liquid, such as titanium, zirconium, vanadium, and niobium, also have a

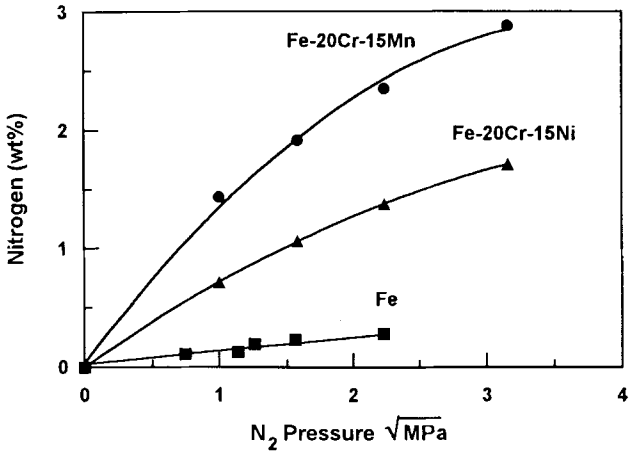

Fig. 1 Nitrogen concentration in liquid iron-base alloys at 1600 °C as a function of alloy additions and N_2 overpressure. Source: Ref 4

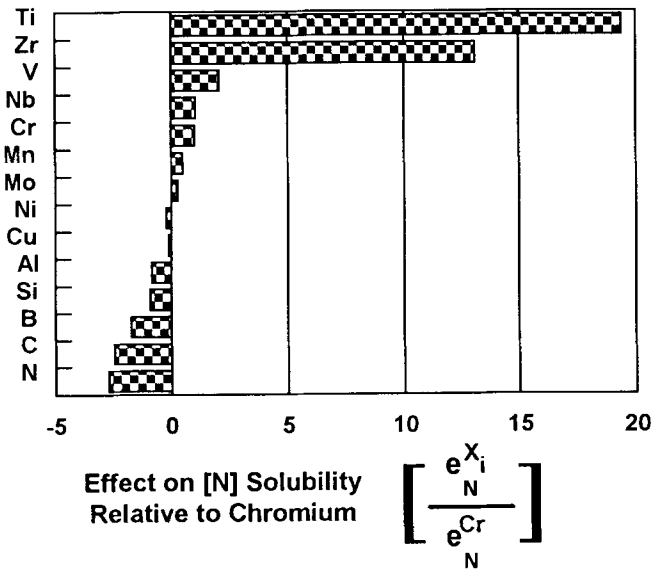

Fig. 2 Effect of alloy additions on nitrogen solubility in iron at 1600 °C, normalized to the effect of chromium. A negative number indicates a reduction in the nitrogen solubility with the alloy addition.

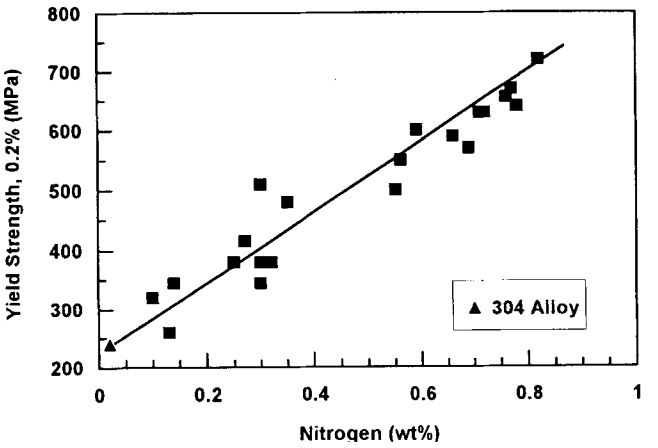

Fig. 3 Effect of nitrogen concentration on YS of austenitic stainless steels. Source: Ref 7-13

strong tendency to form nitrides. Therefore, their use is limited, unless the intent is to produce an alloy containing nitrides. Dispersion-strengthened alloys and materials for wear applications can be produced in this way. Chromium, on the other hand, not only significantly increases nitrogen solubility in liquid iron, but it does so with a lesser tendency (compared to titanium, zirconium, vanadium, and niobium) to form nitrides in the solid state.

Nitrogen Solid-Solution Strengthening

Substitutional elements that stabilize the ferrite structure (tungsten, molybdenum, vanadium, silicon, and chromium) have a small positive effect on yield strength (YS), whereas austenite-stabilizing elements (copper, cobalt, manganese, and

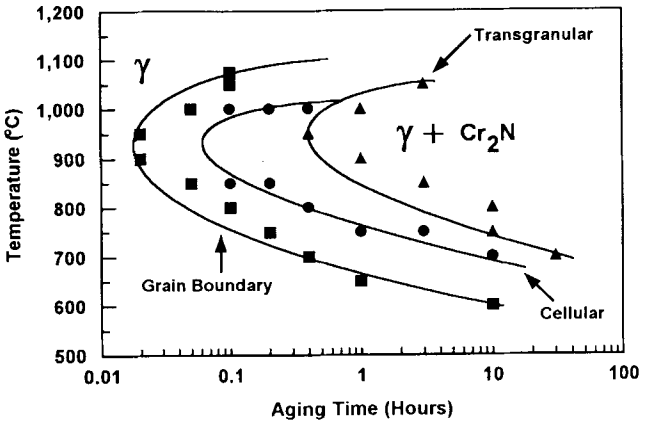

Fig. 4 TTP curves for grain-boundary, cellular, and transgranular Cr_2N precipitation in alloy SS2. Source: Ref 14

nickel) have little effect or, in the case of nickel, a negative effect. Interstitial elements (nitrogen, carbon, and boron) increase the strength of austenitic stainless steels much more than substitutional elements, and nitrogen is more effective than any other element in this regard (Ref 6). The powerful effect of nitrogen on increasing flow stress is illustrated in Fig. 3, where YS is plotted as a function of increasing nitrogen concentration for a variety of austenitic stainless steels (Ref 7-13).

1.3 *Effects of Nitrogen on Mechanical Properties*

Although alloys in which all of the nitrogen is present interstitially in solid solution have excellent tensile and impact properties, they are susceptible to embrittlement after aging in the temperature regime where nitride precipitation occurs. Nitrides can have a seriously detrimental effect on plasticity during the dynamic straining of impact testing and a lesser, but significant, effect on tensile ductility.

Simmons et al. (Ref 14) determined the effects of isothermal aging at 700 and 900 °C on the Cr_2N precipitation characteristics (i.e., morphologies and kinetics) and impact toughness of SS1. The tensile properties of this alloy are discussed in section 1.3.2. The thermal stability and time-temperature-precipitation (TTP) curves of this material are shown in Fig. 4.

1.3.1 Impact Toughness

Isothermal aging of SS1 at 700 and 900 °C results in low-energy room-temperature impact properties, as shown in Fig. 5. Embrittlement results from grain-boundary precipitation of Cr_2N nitrides at 700 °C and from both grain-boundary and cellular Cr_2N precipitation at 900 °C. Increased aging at 700 °C, causing increased nitride coverage of the grain boundaries, results in decreasing impact energies, leading to 100% intergranular fracture after less than 3 h of aging. For short aging times at 900 °C, intergranular fracture dominates, but after longer aging, fracture is mixed mode. Transgranular fracture after aging at 900 °C occurs by decohesion of austenite matrix/Cr_2N lamellae interfacial regions. Similarly, fractographic evidence suggests that fracture at grain boundaries, and through regions of cellular precipitation, is dominated by deco-

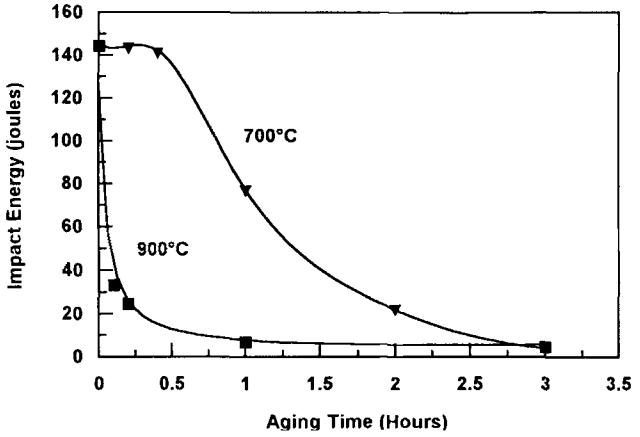

Fig. 5 Impact toughness of SS2 alloy as a function of isothermal aging time at 700 and 900 °C. Source: Ref 14

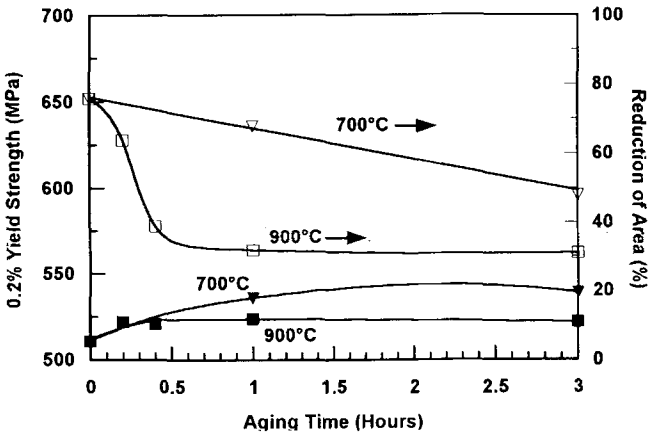

Fig. 6 Effect of isothermal aging on YS and tensile ductility of SS2 alloy, measured by percentage of reduction of area. Open symbols correspond to percentage of reduction of area curves.

Table 1 Chemical compositions of alloys SS1 and SS2

	Composition, wt%							
Alloy	Cr	Mn	Ni	Mo	Si	N	C	Fe
SS1	19.3	5.2	5.2	2.9	0.86	0.69	0.024	bal
SS2(a)	16.2	7.1	4.9	...	0.49	0.06	0.072	bal

(a) Base composition of type 201 stainless steel is used as the master alloy to make SS2 high-nitrogen steels.

hesive failure between the austenite and Cr_2N, and not by brittle fracture of the nitrides.

1.3.2 Tensile Properties

The effects of isothermal aging at 700 and 900 °C on the YS (0.2% offset method) and ultimate tensile strength (UTS) of SS1 are shown in Fig. 6. The presence of grain-boundary and cellular precipitates has little effect on the YS and UTS of the alloy, which are dominated by the properties of the matrix. However, the tensile ductility is significantly affected by aging. At the onset of tensile instability (i.e., necking), the fracture process is dominated by the presence of the precipitates.

These results correlate well with impact toughness results on the same alloy, and also with research conducted by Chandra Holm et al. (Ref 15). In their work the toughness of a cold-worked high-nitrogen (0.58 wt%) stainless steel was observed to decrease significantly with aging at temperatures between 500 and 800 °C.

2. Experimental Procedures

2.1 *Materials and Heat Treatment*

The chemical compositions of the two stainless steel alloys used in this study are listed in Table 1. Alloy SS1 was produced using the pressurized electroslag-remelting process described elsewhere (Ref 16). The material was solution annealed at 1150 °C for 2 h, followed by water quenching. Isothermal aging of solution-annealed material was done at 900 °C for times ranging from 0.1 to 10 h. A second ingot was solution annealed (as before) and cold worked 20% by rolling. The solution-annealed, cold-worked (SA/CW) samples were then aged according to the conditions previously described.

Alloy SS2 is based on the composition of type 201 stainless steel. The type 201 alloy was remelted in a hot isostatic press under a 200 MPa N_2 overpressure. The alloy was held in the liquid state for 4 h at 1650 °C and then furnace cooled to 1000 °C at 200 MPa pressure at a rate of approximately 20 °C/min. At this point in the solidification sequence, the N_2 pressure is reduced to atmosphere and the ingot is cooled to room temperature at 20 °C/min. The resultant ingot had a concentration gradient in nitrogen ranging from a high of 3.60 wt% N at the top to a low of 0.70 wt% N at the bottom. The nitrogen concentrations and corresponding matrix phases are shown in Table 2.

2.2 *Analytical Characterization and Microscopy*

The total nitrogen concentration of each alloy was determined using the inert gas-fusion technique. A Leco Model TC 436 (Leco Corp., St. Joseph, MI) nitrogen-oxygen determinator was used. Interstitial nitrogen concentration analysis was accomplished using Kjeldahl analysis. As-cast, nitrogen-containing stainless steel specimens were dissolved in 1:1 HCl solution in order to differentiate the nitrogen in solution from the nitrogen found in CrN. This is possible because CrN is insoluble in this solution.

The crystal phases present in the alloys were identified using x-ray diffraction (CuK_α radiation). The samples were prepared for metallographic examination using standard polishing

Table 2 Nitrogen concentration, phases, and phase morphologies for alloy SS2

Nitrogen content, wt%	Matrix phases	Phase morphology
0.70	γ	Primary dendrites, single-phase material
	Cr_2N	Cellular precipitation at grain boundaries
1.07	γ	Primary dendrites
	Cr_2N	Cellular precipitation at grain boundaries
1.50	γ	Primary dendrites
	Cr_2N	Isolated regions of cellular precipitation
	CrN	Interdendritic precipitation, microprecipitates
1.93	γ	Primary dendrites
	Cr_2N	Cellular precipitation
	CrN	Interdendritic precipitation, microprecipitates
2.95	γ	Primary dendrites
	Cr_2N	Cellular precipitation
	CrN	Interdendritic precipitation, microprecipitates
3.60	γ	Primary dendrites
	CrN	Interdendritic precipitation

procedures. The microstructures were characterized using both optical microscopy and scanning electron microscopy (SEM) after etching with one of the following solutions: (1) 10 mL HNO_3, 10 mL HCl, 10 mL glacial acetic acid, and two drops of glycerol; or (2) electrolytically with 10% oxalic acid.

Scanning electron microscopy was performed on all abraded samples (both SiC and garnet abrasives were used). Micrographs of the wear surfaces were obtained using both secondary and backscattered electron imaging (SEI and BEI, respectively).

Vickers hardness measurements (1 kg load, 30 s dwell time) were performed for each specimen. A total of 8 and 12 indentations were made and measured on each sample.

2.3 *Abrasive Wear Testing*

The abrasive wear tests performed in this study utilized the pin-on-drum apparatus pictured in Fig. 7, designed and built at the U.S. Bureau of Mines. This is a comparative test that can be used to determine the abrasive wear resistance of a wide range of materials (Ref 17). The pin-on-drum abrasive wear test involves high-stress, two-body abrasion, in which one end of a cylindrical pin specimen is moved over an abrasive paper, causing abrasion of the specimen and crushing of the fixed abrasive grains. This test is designed to simulate the abrasive wear processes that occur during the crushing and grinding of ore.

In this study both 150-grit garnet and 600-grit SiC were used to determine the abrasive wear resistance of the stainless steel alloys. The 150-grit garnet abrasive corresponds to an abrasive particle size of between 80 and 100 μm. The 600-grit SiC abrasive paper has an abrasive particle size of between 17 and 20 μm (Ref 18). Two sizes of abrasive particles were selected because it was noted that the size of the garnet abrasive approached, and in some instances exceeded, the size of the microstructural features in the stainless steels. Consequently, a smaller abrasive particle size was used to assess the effect of microscopic structural features on wear resistance. For tests performed on garnet, the 6.35 mm diam pin was pressed against the drum with a normal force of 66.7 kg. This corresponds to a 2.11 MPa pressure on the surface of the pin. For those samples tested on SiC, the normal force was reduced to 41.8 kg. In this case, the pressure on the pin was 1.32 MPa. The pin was rotated at a peripheral speed of 5.65×10^{-3} m/s (17 rev/min), while the drum rotated at a speed of 4.5×10^{-2} m/s (1.7 rev/min). The wear path was 1.6 m per drum revolution. Pin-on-drum tests were performed on each alloy using 600-grit SiC. Selected samples were also abraded on the 150-grit garnet. After a break-in cycle of four revolutions, wear data were collected for eight revolutions on the SiC and for two, four, and eight revolutions on the garnet. Five sets of tests were performed on the samples abraded on SiC. Two sets of tests were performed at each specified revolution for the samples abraded on the garnet.

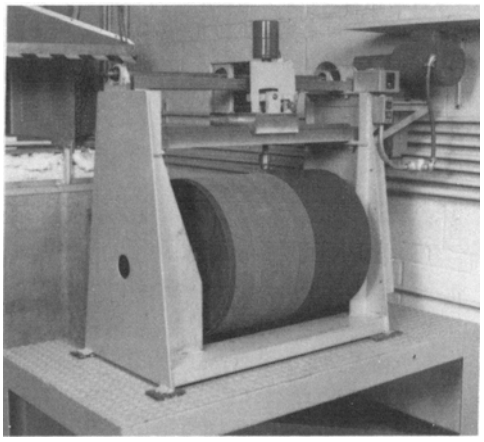

Fig. 7 Pin-on-drum wear-testing machine

The pin-on-drum wear test of a material requires two runs—one on the test specimen and one on a standard specimen. After the test specimen has been abraded, a standard specimen is run for the same number of drum revolutions, with its track between the tracks left by the test specimen to create alternating wear tracks for the standard and test specimens. The standard material is a low-alloy steel, ASTM 514, with a hardness of 269 HB. Standard specimen wear is used to correct for small variations in the effective abrasiveness of the abrasive cloth from lot to lot and within a given lot.

The corrected abrasive wear value of a test specimen for a given abrasive type under a given load is reported as a volume loss per unit wear path and is obtained from

$$W_c = C\frac{W_x\, l}{S_x\, \rho} \qquad \text{(Eq 1)}$$

where W_c is the corrected wear rate (mm^3/m); W_x is the mass loss of the test specimen during an abrasion test of a fixed number of revolutions (any mass units); S_x is the mass loss of the standard specimen during an abrasion test of the same number

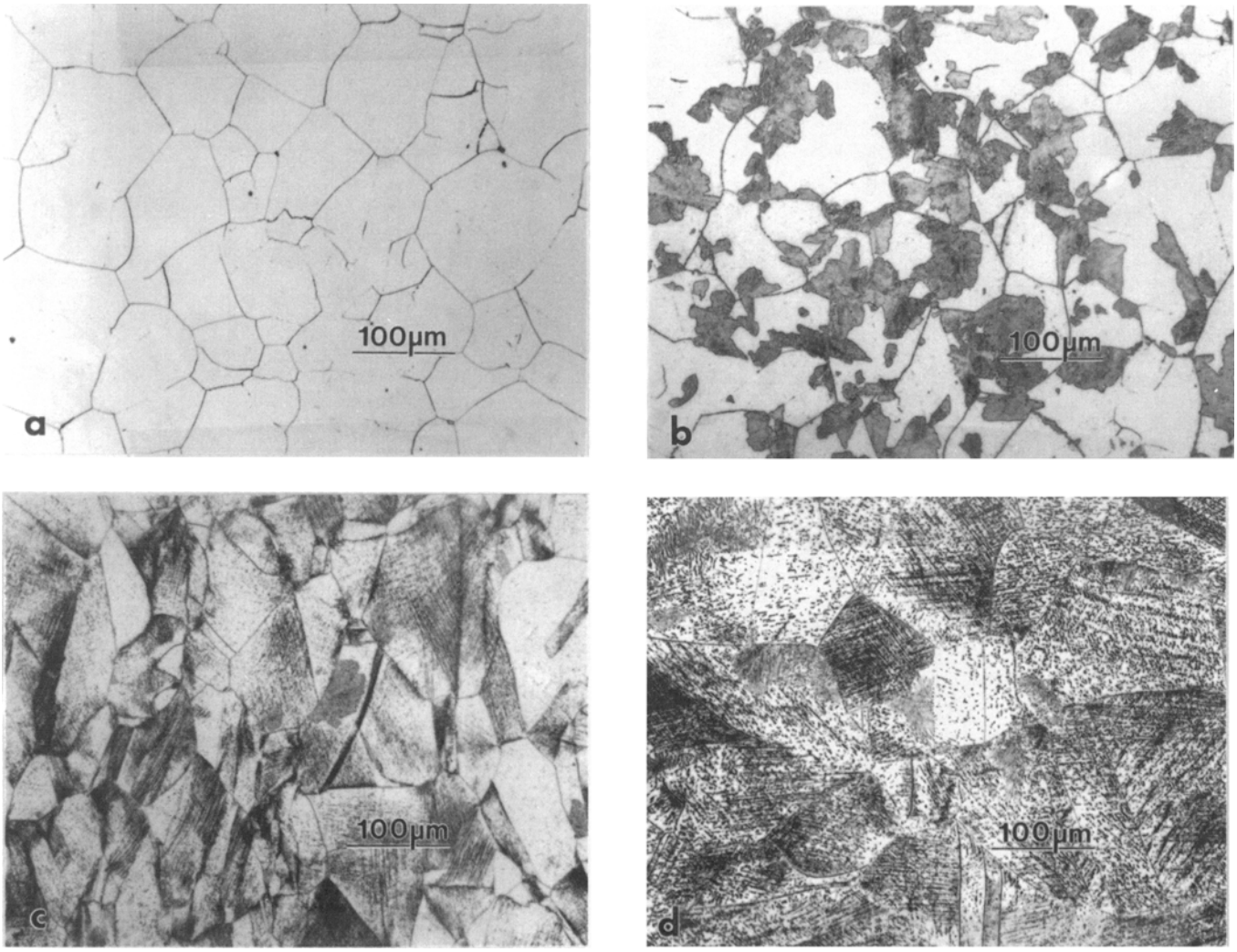

Fig. 8 Microstructures typical of alloy SS1 (a) annealed at 1150 °C for 2 h and (b) after subsequent isothermal aging at 900 °C for 1 h. Cr_2N precipitate morphologies developed in cold-worked (cold rolled 20%) alloy SS1 isothermally aged at 900 °C for (c) 1 h and (d) 10 h.

of revolutions (same mass units of W_x); C is the pin-on-drum abrasive wear constant for a given abrasive, pin load, and standard material; and ρ is the density of the test material (mg/mm^3). The abrasive wear constant, C, has been determined for both abrasive types and grit sizes from a history of several hundred tests: for the 150-grit garnet, C_g is 10.098 mg/m; for the 600-grit SiC, C_{SiC} is 2.500 mg/m. The density of the stainless steels was taken to be 7.94 mg/mm^3. The corrected wear value reflects the intrinsic wear properties of the test material, not a ratio between the test material and the standard material.

3. Results

3.1 *Microstructures*

3.1.1 Alloy SS1

Microstructural features of SA SS1, and samples heat treated at 900 °C, are illustrated in the optical micrographs shown in Fig. 8. The SA alloy does not contain nitrides, because all of the nitrogen can be dissolved interstitially in the austenite matrix by annealing at temperatures above 1100 °C. The basic austenite grain structure of the material is shown in Fig. 8(a). Aging the SA alloy at 900 °C results in the rapid precipitation of Cr_2N at grain boundaries, followed by cellular precipitation and finally, at long aging times, by transgranular Cr_2N precipitation. Grain-boundary precipitate coverage was significant for aging at 900 °C for times as short as 0.1 h, with nearly 100% of the grain boundaries containing precipitates. The nitride density on the boundaries increased with increasing aging time. The cellular precipitate morphologies formed in the SS1 material are illustrated in Fig. 8(b). Cellular precipitation of Cr_2N occurs by the decomposition of the supersaturated austenite matrix (γ_1) to a lamellar structure consisting of an austenite matrix with an equilibrated composition (γ_2), that is, lower nitrogen and chromium contents, and Cr_2N. The reaction can be described as $\gamma_1 \rightarrow \gamma_2 + Cr_2N$ (Ref 18). Cellular precipitation products in this reaction have a morphology that is very similar to pearlite found in carbon steels. Cellular precipitate ($\gamma_2 + Cr_2N$) volume fractions increase with increased aging time at 900 °C and reach 40% after 3 h. The volume fraction of trans-

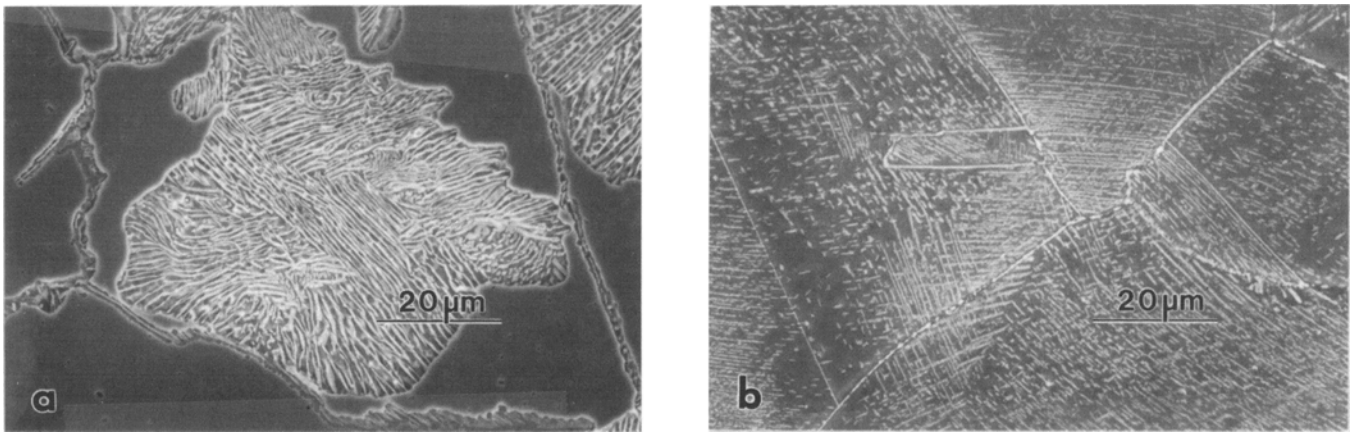

Fig. 9 Secondary electron micrographs showing Cr_2N morphologies present in alloy SS1 after aging of (a) annealed material at 900 °C and (b) cold-worked material at 900 °C. Note the transgranular needlelike Cr_2N produced in cold-worked material compared to cellular growth in annealed material.

granular precipitates formed in SA alloys is very low, because precipitate nucleation within the virtually defect-free matrix is not favored.

Cold working of the SS1 material by cold rolling introduces a high density of defects (e.g., deformation twins and a high density of dislocations present within concentrated slip bands) and produces preferred sites for precipitate nucleation within the matrix. Consequently, subsequent aging of the cold-rolled material at 900 °C results in a rapid increase in the kinetics of grain-boundary and transgranular Cr_2N precipitation, while precipitation by cellular decomposition of the austenite is retarded. The resulting nitride morphologies are shown in Fig. 8(c) and (d).

The lamellar nature of the cellular precipitation products formed in SA alloys aged at 900 °C is shown in the SEI micrograph of Fig. 9(a). The transgranular regions of the SA/CW-aged alloy are dominated by the presence of the needlelike transgranular Cr_2N precipitates shown in Fig. 9(b).

3.1.2 Alloy SS2

Microstructural evolution in the as-cast, high-nitrogen SS2 stainless steel is quite different from the thermomechanically worked SS1 alloy. Precipitate formation in the as-cast SS2 alloy was influenced by the local nitrogen content present in the solidifying liquid as well as segregation caused by the primary austenitic solidification and resulting solute partitioning. Austenite was the primary solidification phase for all of the nitrogen compositions studied, and increasing nitrogen concentrations resulted in increasing amounts of Cr_2N and CrN. The formation of the Cr_2N lamellar structure occurs in the solid state by cellular decomposition of the supersaturated austenite and is the primary nitride structure formed at lower nitrogen contents. As the nitrogen content of the alloy increases, dendritic solidification of CrN occurs within the interdendritic regions of the primary austenite. The volume fraction of the dendritic CrN increases with increasing nitrogen concentration. The typical nitride structures formed as a function of increasing nitrogen are illustrated in the optical micrographs of Fig. 10.

The 0.70 wt% N material solidified entirely as austenite, with Cr_2N cellular precipitation taking place at grain boundaries during cooling due to the decrease in solid solubility of nitrogen in the austenite with decreasing temperature (Fig. 10a). The 1.07 wt% N contained a high volume fraction of the cellular precipitate products, with very little untransformed primary austenite remaining (Fig. 10b). A small amount of interdendritic CrN was present in the 1.50 wt% N material, which also contained submicron CrN precipitates in the matrix adjacent to the interdendritic CrN (Fig. 10c). Only isolated regions of cellular Cr_2N were present in this alloy. Alloy SS2 with 1.93 wt% N contained increasing amounts of interdendritic CrN, a large volume fraction of cellular Cr_2N, and some CrN microprecipitates (Fig. 10d). The microstructure of the alloy with 2.95 wt% N was similar to the 1.93 wt% N material, except that the former contained higher volume fractions of interdendritic CrN dendrites and cellular Cr_2N, as would be expected from the increased nitrogen in this region (Fig. 10e). The alloy with 3.60 wt% N contained significant interdendritic CrN, and the primary austenite dendrites were essentially fully transformed to cellular decomposition products (Fig. 10f).

3.2 *Hardness*

The Vickers hardnesses of the SA-aged samples are given in Table 3. The SA alloy had a hardness of 229 kg/mm^2. Subsequent aging caused an overall gradual increase in hardness until a maximum was reached after 10 h at 900 °C (264 kg/mm^2). The increase in hardness with aging at 900 °C was small and due to Cr_2N matrix precipitates.

Vickers hardness results for SS1 SA/CW-aged samples are given in Table 4. A hardness value of 355 kg/mm^2 was obtained for the SA/CW alloy. Aging at 900 °C caused an immediate decrease in hardness to approximately 315 kg/mm^2 after just 0.1 to 0.2 h. The hardness continued to decrease to 294 kg/mm^2 after aging at 900 °C for 10 h.

For the SS2 cast alloys (Table 5), the hardness of the matrix increased as the total volume fraction of Cr_2N and CrN precipitates increased. Hardness of the as-received (AR) type 201 was 150 kg/mm^2. As more nitrogen was incorporated into the cast alloy, matrix hardness increased to a maximum of 353 kg/mm^2

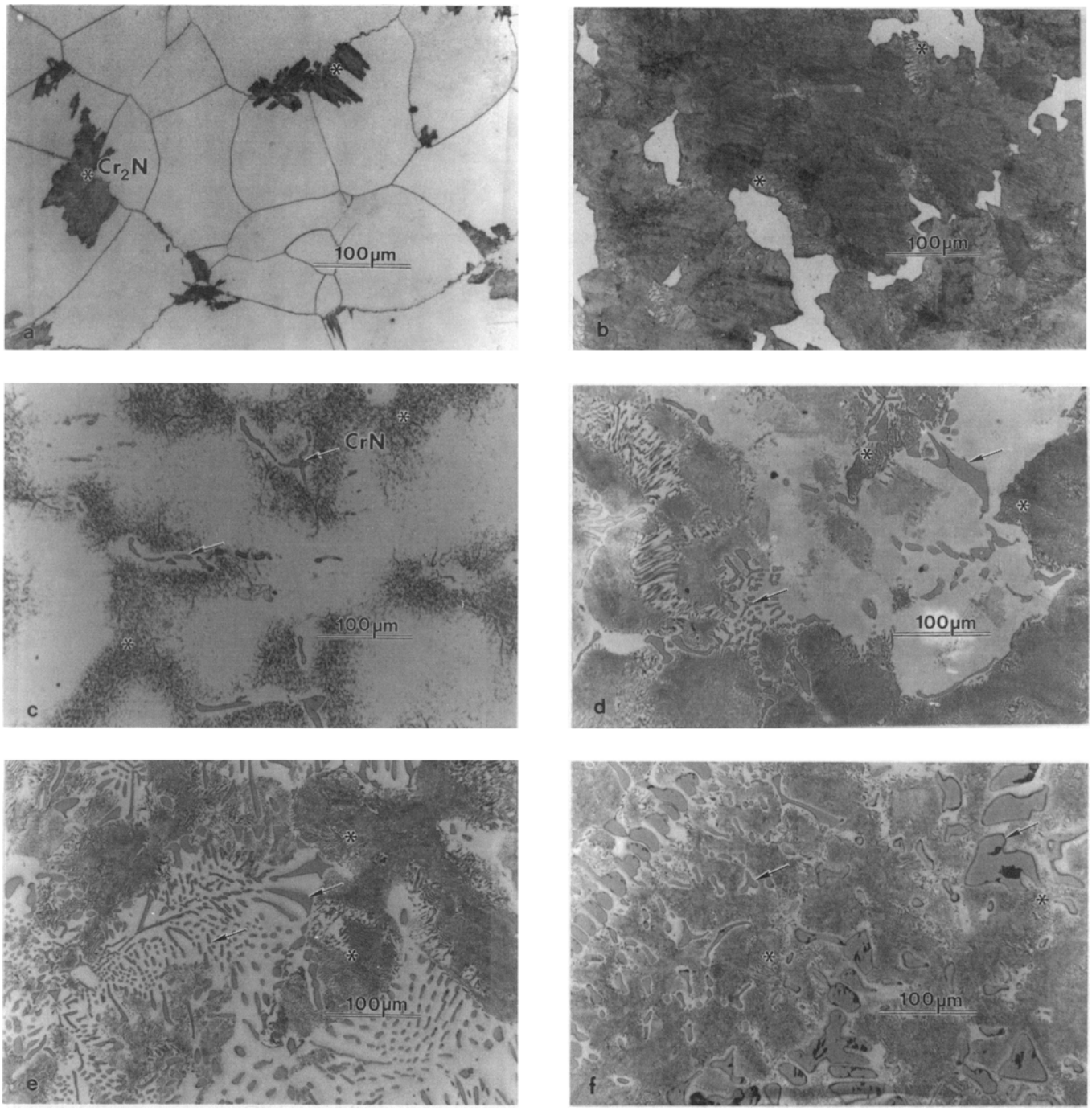

Fig. 10 Optical micrographs of alloy SS2. (a) 0.70 wt% N. (b) 1.07 wt% N. (c) 1.50 wt% N. (d) 1.93 wt% N. (e) 2.95 wt% N. (f) 3.60 wt% N. The asterisks denote cellular precipitation of Cr_2N. The arrows denote CrN dendrites.

for sample SS2(6). For alloy SS2(C + N), containing 2.01 wt% C in addition to nitrogen, a matrix hardness of 431 kg/mm^2 was measured.

3.3 *Abrasive Wear*

The results of the pin-on-drum abrasive wear tests of alloys SS1 and SS2 are given in Tables 3 to 7. The information on abrasive wear is presented in three ways. The first representation of the wear of the material is in terms of mass loss, which is simply the amount of material removed during the test per meter of abrasive traversed (i.e., W_x / S_x). This value is "corrected" using the abrasive wear constant, C, for the appropriate abrasive cloth (i.e., CW_x / S_x). Consequently, abrasive wear is represented as the ratio of wear of a specimen material to a standard material in terms of mass loss per unit sliding distance (i.e., mg/m). The second representation of abrasive wear

Table 3 Abrasive wear of alloy SS1 on 600-grit SiC
Solution annealed and aged at 900 °C

Alloy SS1 heat treatment	Observed microstructure	CW_x/S_x, mg/m	W_c, mm^3/m	W_c^{-1}, m/mm^3	DPH, kg/mm^2
SA	γ (matrix)	1.703 ± 0.083	0.214 ± 0.010	4.67 ± 0.22	229
SA + 900 °C/6 min		1.690 ± 0.093	0.213 ± 0.012	4.69 ± 0.26	231
SA + 900 °C/12 min	γ (matrix) Grain-boundary Cr_2N Cellular Cr_2N	1.683 ± 0.123	0.212 ± 0.015	4.72 ± 0.33	225
SA + 900 °C/24 min		1.713 ± 0.068	0.216 ± 0.009	4.63 ± 0.19	243
SA + 900 °C/60 min		1.703 ± 0.078	0.214 ± 0.010	4.67 ± 0.22	259
SA + 900 °C/180 min	γ (matrix) Grain-boundary Cr_2N Cellular Cr_2N	1.685 ± 0.025	0.212 ± 0.003	4.72 ± 0.07	255
SA + 900 °C/600 min	Transgranular Cr_2N	1.670 ± 0.030	0.210 ± 0.004	4.76 ± 0.09	264

Table 4 Abrasive wear of alloy SS1 on 600-grit SiC
Solution annealed, cold worked 20%, and aged at 900 °C

Alloy SS1 heat treatment	Observed microstructure	CW_x/S_x, mg/m	W_c, mm^3/m	W_c^{-1}, m/mm^3	DPH, kg/mm^2
SA/CW 20%	γ (matrix)	1.728 ± 0.018	0.218 ± 0.002	4.59 ± 0.04	355
SA/CW + 900 °C/6 min		1.733 ± 0.023	0.218 ± 0.003	4.59 ± 0.06	313
SA/CW + 900 °C/12 min	γ (matrix) Grain-boundary Cr_2N Transgranular Cr_2N	1.745 ± 0.040	0.220 ± 0.005	4.55 ± 0.10	317
SA/CW + 900 °C/24 min		1.738 ± 0.035	0.219 ± 0.004	4.57 ± 0.08	308
SA/CW + 900 °C/60 min		1.738 ± 0.015	0.219 ± 0.002	4.57 ± 0.04	305
SA/CW + 900 °C/180 min	Transgranular Cr_2N (elongated needles) Isolated cellular Cr_2N	1.723 ± 0.055	0.217 ± 0.007	4.61 ± 0.15	307
SA/CW + 900 °C/600 min		1.653 ± 0.050	0.208 ± 0.006	4.81 ± 0.14	294

Table 5 Abrasive wear of alloy SS2 on 600-grit SiC
Hot isostatically pressed under 200 MPa N_2 pressure

Alloy designation	Nitrogen (solution), %	Nitrogen (CrN precipitate), %	Nitrogen (total), %	CW_x/S_x, mg/m	W_c, mm^3/m	W_c^{-1}, m/mm^3	DPH, kg/mm^2
SS2(AR)	0.06(2)	0.00(3)	0.06(5)	1.845 ± 0.003	0.232 ± 0.000	4.31 ± 0.01	150
SS2(1)	0.68	0.02	0.70	1.853 ± 0.003	0.233 ± 0.000	4.29 ± 0.01	227
SS2(2)	0.90	0.17	1.07	1.803 ± 0.010	0.227 ± 0.001	4.41 ± 0.02	312
SS2(3)	0.73	0.77	1.50	1.758 ± 0.005	0.221 ± 0.001	4.53 ± 0.01	322
SS2(4)	0.67	1.26	1.93	1.680 ± 0.010	0.212 ± 0.001	4.72 ± 0.03	339
SS2(5)	0.24	2.71	2.95	1.560 ± 0.015	0.196 ± 0.002	5.10 ± 0.05	346
SS2(6)	0.17	3.43	3.60	1.425 ± 0.040	0.179 ± 0.005	5.59 ± 0.16	353
SS2(C + N)	0.13	2.81	2.94	1.325 ± 0.003	0.167 ± 0.000	5.99 ± 0.01	431

is given by the wear rate, W_c, which is the density-corrected value of the wear rate calculated above (i.e., $CW_x / \rho S_x$), which represents the intrinsic wear behavior of the material. The units of W_c are in volume of material lost to abrasion per unit distance of abrasive traversed (i.e., mm^3/m). The third way to represent abrasive wear is through the reciprocal of the wear rate, W_c^{-1}; this number is a measure of the wear resistance of the material (m/mm^3). The utility of using wear resistance as a measure of abrasive wear is that the higher the number, the more resistant the alloy is to wear processes.

3.3.1 Abrasive Wear on 600-Grit SiC

Table 3 gives the abrasive wear results for the SA-aged SS1 alloy abraded on 600-grit SiC. It can be seen that changes in microstructure due to the aging sequence have little effect on the abrasive wear of the material. There is a very small increase in the wear resistance for the SA specimen aged at 900 °C for 600 min. Although small in magnitude, the increase in wear resistance with aging time was a real effect.

Table 4 provides data on the wear of the SA/CW-aged SS1 alloy. In general, the wear resistance of this alloy was slightly lower than that of the SA-aged material, except at the very longest time (i.e., SA/CW + 900 °C/600 min).

The results of pin-on-drum abrasive wear for alloy SS2 are given in Table 5. Several interesting trends are apparent. First, the overall abrasive wear of the material is controlled by the CrN precipitate. As the number and size of this phase increase, the wear resistance also increases. The highest wear resistance belohgs to the specimen containing the largest number of coarse CrN precipitates. The trend of increasing wear resis-

Table 6 Abrasive wear of alloy SS1
150-grit garnet; tested at two, four, and eight revolutions

Alloy designation	CW_s/S_s, mg/m	W_c, mm^3/m	W_c^{-1}, m/mm^3
SS1(SA)	6.957 ± 0.135	0.876 ± 0.017	1.14 ± 0.02
SS1 (SA + 900 °C/600 min)	7.517 ± 0.219	0.947 ± 0.028	1.06 ± 0.03
SS1 (SA/CW 20%)	7.295 ± 0.069	0.919 ± 0.009	1.09 ± 0.01
SS1 (SA/CW + 900 °C/600 min)	7.411 ± 0.090	0.933 ± 0.011	1.07 ± 0.01

Table 7 Abrasive wear of alloy SS2
150-grit garnet; tested at two, four, and eight revolutions

Alloy designation	CW_s/S_s, mg/m	W_c, mm^3/m	W_c^{-1}, m/mm^3
SS2(AR)	7.238 ± 0.039	0.912 ± 0.005	1.10 ± 0.01
SS2(1)	7.143 ± 0.003	0.900 ± 0.000	1.11 ± 0.00
SS2(2)	7.116 ± 0.090	0.896 ± 0.011	1.12 ± 0.01
SS2(3)	7.098 ± 0.030	0.894 ± 0.004	1.12 ± 0.01
SS2(4)	6.957 ± 0.064	0.876 ± 0.008	1.14 ± 0.01
SS2(5)	6.871 ± 0.039	0.865 ± 0.005	1.16 ± 0.01
SS2(6)	6.047 ± 0.052	0.762 ± 0.007	1.31 ± 0.01
SS2(C + N)	4.877 ± 0.114	0.614 ± 0.014	1.63 ± 0.04

tance with increasing nitrogen is also reflected in the hardness measurements for these alloys. The wear resistance increases concurrently with matrix hardness, and this parallels the increase in nitrogen in the alloy in the form of CrN precipitates.

Also shown in Table 5 is the wear behavior of the SS2(C + N) alloy. This alloy was contaminated with graphite during the remelting cycle. Consequently, it contained Fe_3C in addition to the CrN precipitates. This alloy can be best described as a high-carbon, high-nitrogen steel. The incorporation of carbon in the alloy in the form of Fe_3C dramatically increases both the hardness and the wear resistance of the alloy compared to SS2(5), which contains a similar amount of nitrogen, but no carbon. The increase in wear resistance for SS2(C + N) compared to SS2(5) is approximately 18%. This increase in wear resistance is related to the size of the strengthening phases and the total volume fraction of phases present in the microstructure of SS2(C + N). That is, when the Fe_3C or CrN precipitate is large, wear resistance of the alloy increases. In the case of SS2(C + N), both large Fe_3C and CrN precipitates coexist in the matrix, and they act in concert to improve wear resistance. It has not been possible to determine the effect of each individual phase on wear resistance, because one specimen is insufficient to deduce the extent of the effect.

3.3.2 Abrasive Wear on 150-Grit Garnet

It was expected that the large abrasive particle size of the garnet would obscure minor variations in the wear behavior of the alloys, because the size of the abrasive particle is as large or larger than the Cr_2N precipitates.

For alloy SS1, only the SA, SA + 900 °C/600 min, SA/CW, and SA/CW + 900 °C/600 min specimens were abraded on the 150-grit garnet (Table 6). The wear behavior using this abrasive was totally unexpected. For example, of the four alloys tested, the least amount of wear was exhibited by the SA alloy. The SA alloy also exhibited better wear resistance than the SA/CW sample when tested on SiC. Previously, both the SA and SA/CW samples, heat treated for 600 min at 900 °C, had superior resistance to abrasive wear on SiC than did the non-heat-treated specimens. This trend was not observed for the samples heat treated for 600 min and then abraded on garnet. In this case, the SA specimen had a higher wear resistance than the SA + 900 °C/600 min alloy (i.e., a wear resistance of 1.14 m/mm^3 compared to 1.06 m/mm^3 and showed improvement in wear resistance compared to the SA/CW + 900 °C/600 min specimen (i.e., 1.14 m/mm^3) compared to 1.07 m/mm^3). Finally, both the SA and SA/CW specimens had superior wear resistance when compared to their respective aged counterparts. The trend in wear behavior was opposite of that displayed for the identical specimens tested on SiC.

Table 7 gives the results of alloy SS2 tested on 150-grit garnet. Very little variation in the abrasive wear resistance is seen in these alloys until the CrN precipitate becomes large and "blocky" in alloy SS2(6). For alloys SS2(AR) through SS2(5), the wear resistance increases from 1.10 to 1.16 m/mm^3. Up to this point, the CrN ranges from about 1 to 10 μm in diameter on average. For SS2(6), the CrN precipitates have coarsened significantly (due in large part to the supersaturation on nitrogen in the alloy melt), attaining sizes of up to 50 μm in width. Consequently, there is a significant increase in the abrasive wear resistance of this alloy.

The SS2 alloy contained a large amount of both nitrogen (2.94 wt%) and carbon (2.01 wt%) and exhibited the best wear resistance of all alloys tested. As was the case when tested on the SiC abrasive, the superior wear resistance of SS2(C + N) resulted from the combined high volume fraction of large, hard CrN and Fe_3C precipitates.

4. Discussion

4.1 *Abrasive Wear of SS1*

Alloy SS1 contained only 0.7 wt% N in solution. The SA-aged specimens developed well-defined precipitate morphologies, consisting of either grain-boundary Cr_2N, cellular Cr_2N, transgranular Cr_2N, or a combination of the three. However, the Cr_2N precipitates were generally less than 0.5 μm in width for the thermomechanical treatments used. The abrasive wear of the alloy was similar in all instances when abraded on the 600-grit SiC. These results are shown in Fig. 11 and 12. For both the SA- and SA/CW-aging treatments, 600 min at 900 °C resulted in increased wear resistance. In the case of the SA-aged material, this increase in wear resistance was related to the increase in hardness of the alloy (i.e., the hardness increases from 229 to 264 kg/mm^2). Generally, the higher the hardness of the material, the greater its wear resistance.

Cold working the SA alloy combined with subsequent aging led to a dramatic increase in the hardness of the material (i.e., 355 kg/mm^2). However, there was no corresponding large increase in wear resistance, as would normally be expected. In fact, the SA/CW alloy had a higher wear rate compared to the SA alloy (i.e., 0.218 versus 0.214 mm^3/m), even though the hardness of the SA alloy is much less than that of the SA/CW al-

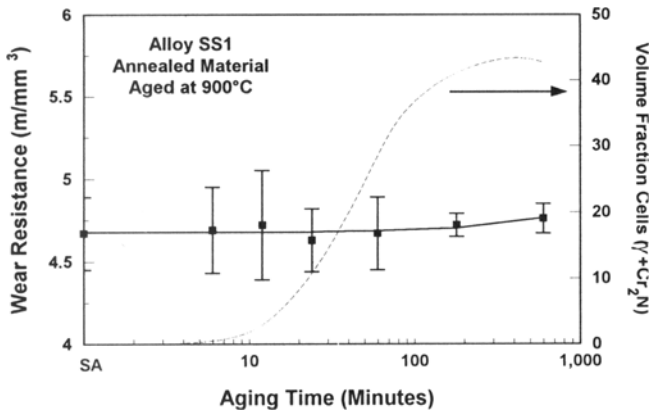

Fig. 11 Wear resistance of alloy SS1 (SA-aged at 900 °C/6 to 600 min) versus aging time. Also included is the volume fraction of cells as a function of aging time.

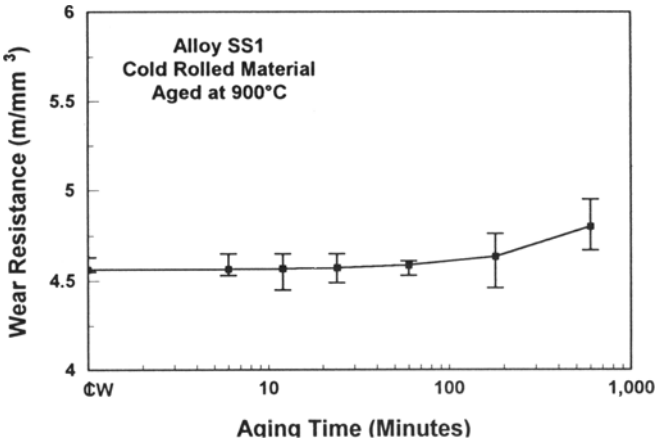

Fig. 12 Wear resistance of alloy SS1 (SA/CW-aged at 900 °C/6 to 600 min) versus aging time

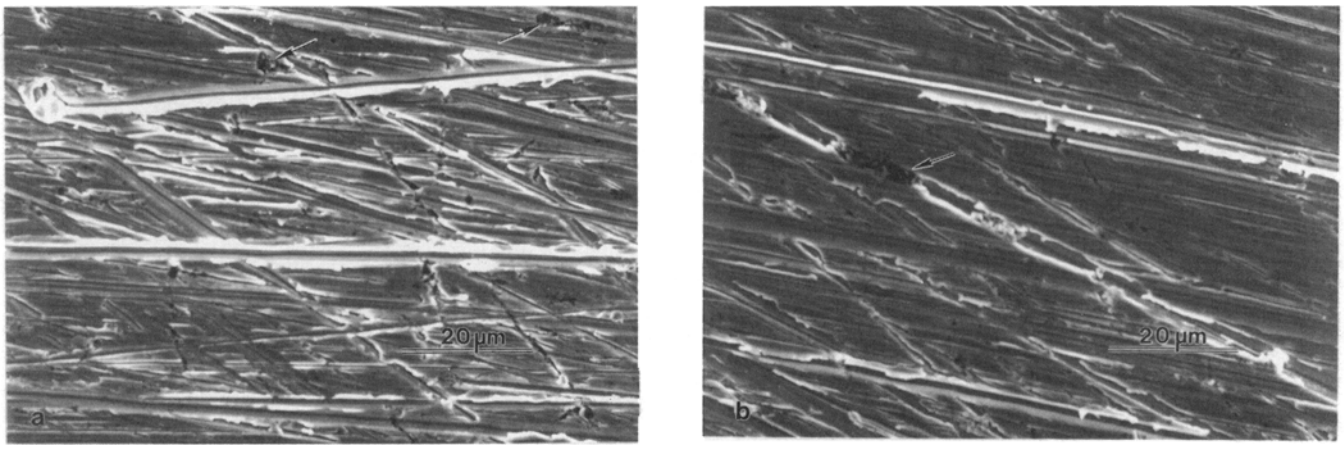

Fig. 13 SiC-abraded wear surface of (a) SA and (b) SA/CW SS1. The arrows highlight an area where microfracture has occurred.

loy. It was noted earlier that aging the SA/CW alloy resulted in a loss in impact toughness and ductility. In addition, fracture in aged specimens occurred at grain boundaries and in regions of cellular precipitation through the decohesive failure between the austenite and Cr_2N. The kinetics of precipitation in these materials is accelerated by the cold work, and, as such, Cr_2N precipitates form at shorter times. The wear rate of the SA/CW alloy may be higher because of a combination of cutting and microfracture. Figure 13 shows typical wear surfaces for the SA and SA/CW alloys. The wear surface shows signs of cutting (note the sharp grooves in the sample) as well as small regions characterized by microfracture (note the arrowed areas). If microfracture is also occurring, then the wear rate will be slightly higher than for cutting alone.

This explanation does not account for the increase in wear resistance after aging for 600 min at 900 °C. However, if the Cr_2N precipitates coarsen because of prolonged aging, then they will contribute to a small decrease in the wear rate because they are harder and wear less rapidly than the matrix.

When these alloys are abraded on garnet, the wear behavior changes completely. For instance, the SA alloy now wears at the lowest rate. Two factors have changed in these tests: the size of the abrasive and the hardness of the abrasive. For steels, the hardness of the abrasive should not be the controlling factor, because both garnet and SiC are significantly harder than steel. This seems to imply that the size of the abrasive particle is important. Because the garnet particles are now much larger than typical microstructural features, the dominant wear mechanism has changed from cutting and microfracture to cutting alone. Consider that the SA alloy is the most ductile and, as such, is plastically deformed and cut during abrasive wear. As the sample is aged, the hardness increases but not the wear resistance. In this case, the wear mechanism probably includes fracture between the austenite and Cr_2N, thereby increasing the wear rate. The SA/CW alloy is harder as a result of the plastic deformation of cold working. However, because this alloy has not been aged, Cr_2N precipitates have not yet nucleated, and thus fracture at the austenite/Cr_2N interface is not a viable wear mechanism. After the material has been aged, the wear rate increases slightly, but it is not significantly different; that is, wear rates overlap. This slight increase may be attributed to decohesive fracture at the austenite/Cr_2N interface.

In summary, the wear behavior of SS1 is little affected by the precipitation of Cr_2N. Although the nitrogen changes the morphology of the microstructure, the size of the Cr_2N precipi-

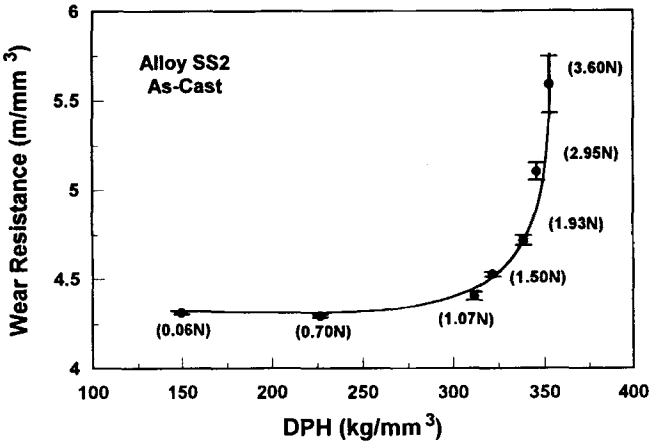

Fig. 14 Wear resistance for alloy SS2 (type 201 stainless steel) versus diamond pyramid hardness (DPH) for alloys with different weight percentages of nitrogen (600-grit SiC abrasive)

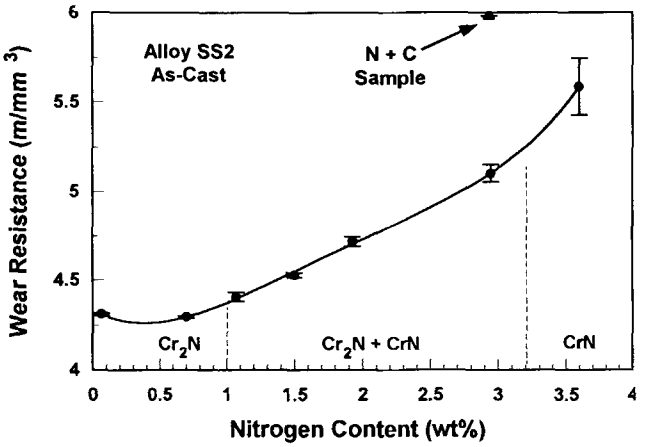

Fig. 15 Wear resistance for alloy SS2 (type 201 stainless steel) versus total nitrogen content (600-grit SiC abrasive)

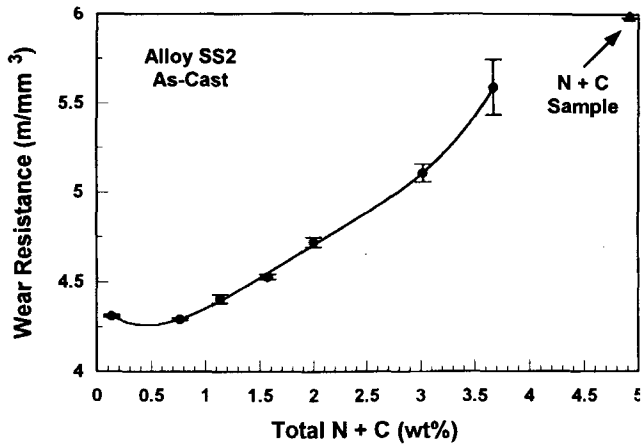

Fig. 16 Wear resistance for alloy SS2 (type 201 stainless steel) versus total nitrogen and carbon content (600-grit SiC abrasive)

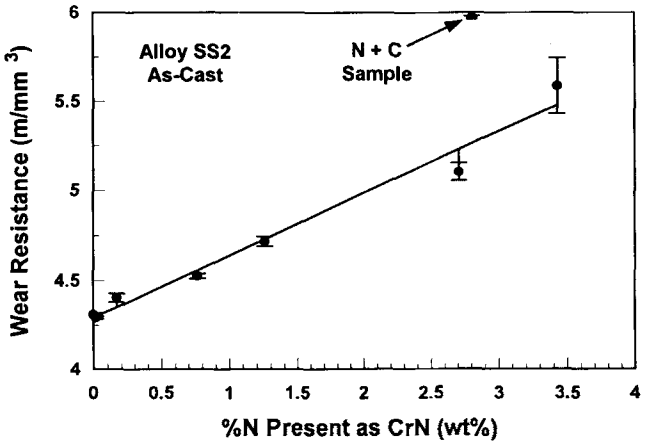

Fig. 17 Wear resistance for alloy SS2 (type 201 stainless steel) versus percentage of nitrogen present in CrN (600-grit SiC abrasive)

tates and their density are insufficient to dramatically improve wear resistance.

4.2 *Abrasive Wear of SS2*

Unlike the SS1 alloy, the wear behavior of SS2 is dramatically affected by the precipitate morphology that forms during the N_2-overpressure remelting process. Significantly more nitrogen is incorporated into the alloy using this technique, and, as previously noted, coarse CrN precipitates nucleate and grow in these cast alloys.

Figure 14 depicts the change in wear resistance of SS2 with hardness. Two points must be mentioned. First, at nitrogen levels of ≥1.07 wt%, the wear resistance of SS2 abraded on 600-grit SiC increases much faster than the hardness. Second, both the hardness and wear resistance of SS2 increase significantly only after nitrogen in excess of that which can be dissolved interstitially becomes available to form chromium nitrides (i.e., Cr_2N and CrN). This would imply that the nitride precipitates are the most important microstructural feature affecting abrasive wear behavior. To better assess the role of the CrN precipitates in the wear process, plots of total nitrogen content versus wear resistance (Fig. 15), total nitrogen and carbon in the alloy versus wear resistance (Fig. 16), and nitrogen in the CrN precipitate versus wear resistance (Fig. 17) were constructed.

Figure 15 shows a gradual increase in the wear resistance as the nitrogen content increases. However, the curve is approximately linear only in the interval between 0.70 and 1.93 wt% N. There is a flat response (i.e., no change in wear resistance with nitrogen) for type 210 and the alloy containing 0.7 wt% N. This implies that total nitrogen in the material is not the wear-controlling factor.

Figure 16 was constructed to assess the possible effect of carbon in the wear process. Like nitrogen, carbon also provides solid-solution strengthening as well as matrix strength through carbide formation. The shape of the curve in Fig. 16 changes only slightly from that shown in Fig. 15, with the linear region now extending from 0.77 to 3.02 wt% (C + N). Included in Fig. 16 is the data point from an alloy that was processed in exactly the same way as SS2, except that it was contaminated with carbon during processing.

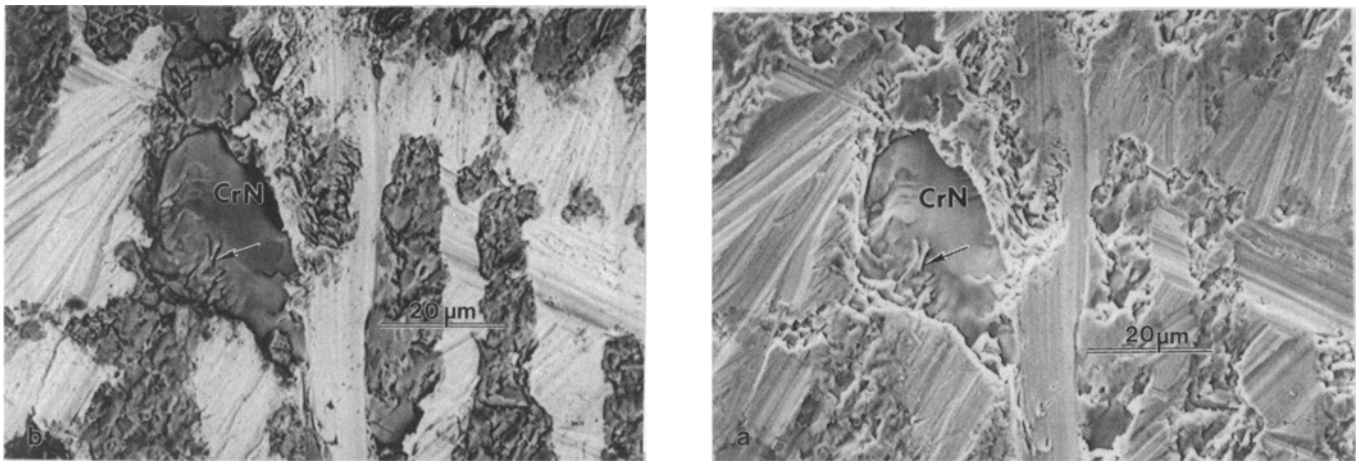

Fig. 18 Garnet-abraded wear surface of alloy SS2(6), with 3.60 wt% N. (a) SEI showing wear scars and CrN precipitates. (b) BEI of the same region highlighting the CrN precipitates. Note that the CrN interrupts the wear scar path.

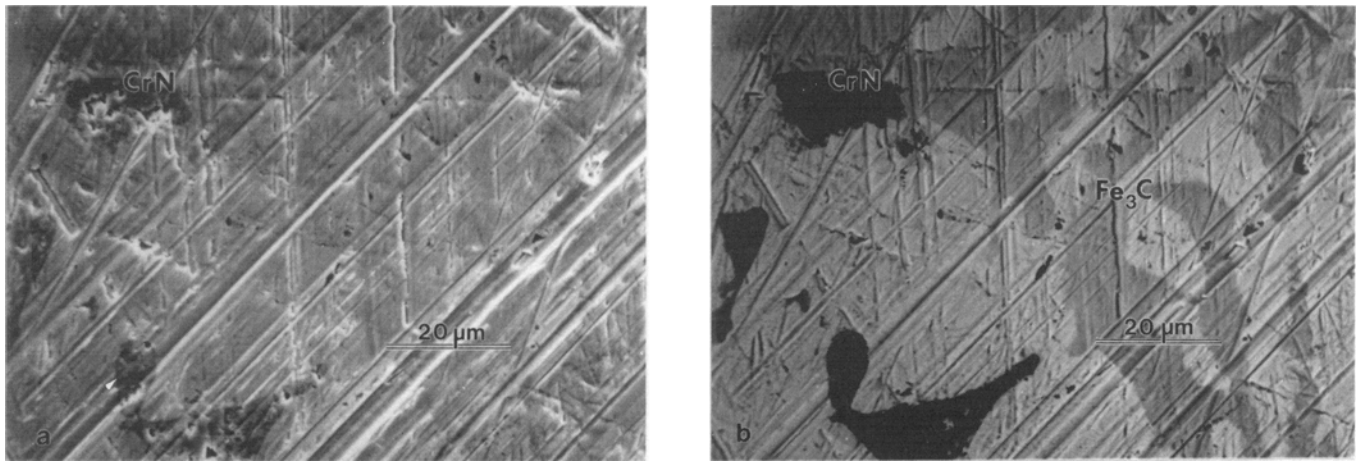

Fig. 19 SiC-abraded wear surface of alloy SS2(C + N). (a) SEI showing wear scars. (b) BEI of same region showing the Fe_3C and CrN phases. The SiC abrasive cuts the Fe_3C; however, wear in the CrN region occurs by microfracture.

Figure 17 is a graph of the nitrogen in the CrN versus wear resistance. The nitrogen in the CrN is calculated by subtracting the Kjeldahl nitrogen (i.e., the interstitial nitrogen in the alloy plus the nitrogen in Cr_2N) from the total nitrogen in the alloy. In this way, the effect of the coarse nitride precipitates (CrN) on wear behavior can be determined. As can be seen, a linear relationship exists between the nitrogen in CrN and wear resistance for all alloys except that contaminated with carbon. A linear least-squares analysis of the data yielded a correlation of 0.988. Given the usual scatter in wear data, this correlation is reasonable. A relation between wear resistance and weight percentage of CrN was obtained:

$$W^{-1} = 4.293 + 0.345(\text{CrNwt\%}) \quad \text{(Eq 2)}$$

It is clear that the CrN precipitates are important in abrasive wear.

The effect that CrN has on the wear process is highlighted in Fig. 18, which shows a portion of the wear surface for SS2(6) abraded on garnet. In Fig. 18(a), wear mechanisms include cutting and microfracture. However, when the same area is examined using backscattered electrons, the CrN precipitates are clearly defined, indicating that the wear mechanism is more complicated. The CrN reduces overall wear because the precipitate is equivalent in hardness to the garnet, deflecting the abrasive particles out of their grooves as the specimen is abraded. As the volume fraction of CrN increases, the garnet rides across the CrN and only grooves the matrix between the precipitates. It is also apparent that CrN fractures during abrasion rather than being cut, because microcracks are visible in many of the CrN precipitates. Therefore, the wear mechanism in SS2 alloys with primary CrN precipitates is one of cutting of the matrix, concurrent with microfracture of the CrN precipitates.

Figure 19 shows the wear surface of the SS2(C + N) alloy abraded on SiC. The SiC abrasive particles are more effective in cutting the matrix, the CrN precipitate, and, in this case, the Fe_3C phase. Principally, cutting and microfracture within the CrN precipitate occur.

Figure 20 highlights the difference in the wear scars during abrasive wear when using garnet instead of SiC on the SS2 al-

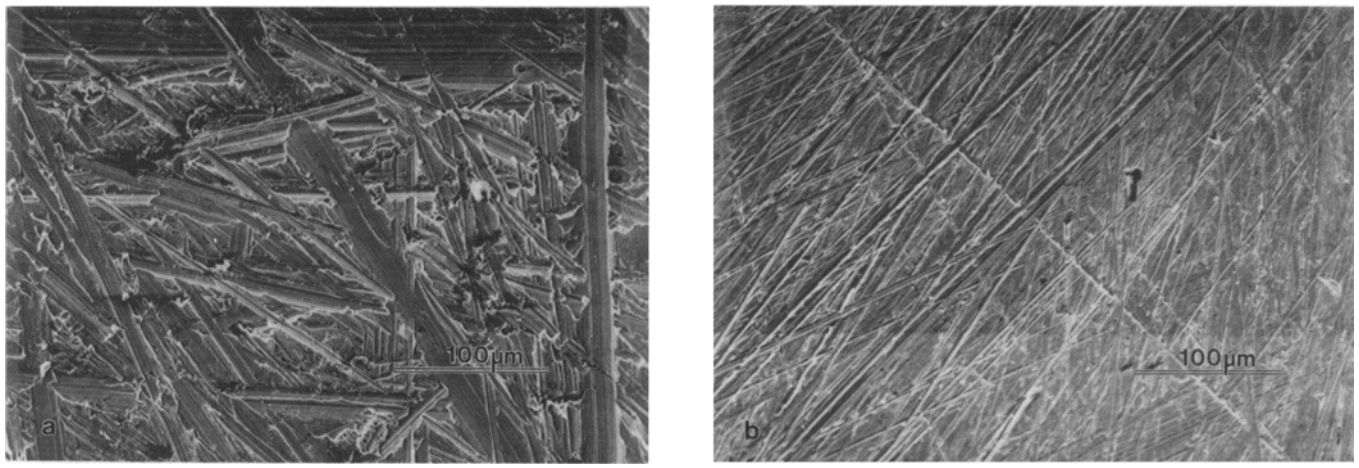

Fig. 20 Scanning electron micrographs of the wear surface of alloy SS2(1) showing the relative size difference of the wear scars from (a) 150-grit garnet and (b) 600-grit SiC

Table 8 Comparison of abrasive wear on various steels
150-grit garnet; average of pin-on-drum tests

Alloy designation	CW_x/S_x, mg/m	W_c, mm^3/m	W_c^{-1} m/mm^3
SS2(C + N)	4.877 ± 0.114	0.614 ± 0.014	1.63 ± 0.04
SS2(6)	6.047 ± 0.052	0.762 ± 0.007	1.31 ± 0.01
SS1(SA)	6.957 ± 0.135	0.876 ± 0.017	1.14 ± 0.02
Type 201	7.238 ± 0.039	0.912 ± 0.005	1.10 ± 0.01
SS1(SA/CW)	7.295 ± 0.069	0.919 ± 0.009	1.09 ± 0.01
1080 rail steel	8.411 ± 0.057	1.073 ± 0.007	0.93 ± 0.01
Type 316	9.035 ± 0.181	1.144 ± 0.023	0.87 ± 0.02
Iron	14.399 ± 0.063	1.832 ± 0.008	0.55 ± 0.00

loys. Very little change in wear rate occurred until the coarse CrN primary dendrites dominated the microstructure, at which point wear resistance increased dramatically. For the alloys strengthened primarily with interstitial nitrogen, abrasive wear is affected more by the size of the abrading particle than by the hardness of the abrasive. Additionally, the overall hardness of the matrix plus precipitate phase is important. In general, the higher the matrix hardness of the alloy, the higher the abrasive wear resistance.

4.3 *Comparison of Abrasive Wear Behavior for Various Steels*

In order to better compare the wear resistance of the high-nitrogen stainless steels to other ferrous materials, collateral tests on several typical irons and steels have been carried out on the 150-grit garnet abrasive. These results are given in Table 8. In comparison to a 1080 rail steel and type 316 stainless steel, the nitrogen-containing stainless steels SS2 and SS1 possessed superior abrasive wear resistance. All the alloys containing nitrogen performed better than the non-nitrogen-containing materials. This result occurs partly because the nitrogen-containing steels have higher YS, UTS, and hardness than do the steels without nitrogen.

5. Summary and Conclusions

Nitrogen has a beneficial effect on the strength and abrasive wear behavior of stainless steels because of changes in the microstructural morphology of the alloys due to nitride precipitation (i.e., Cr_2N and CrN). Specifically, when the nitrogen in the alloy is ≤0.7 wt%, the alloy is strengthened interstitially. For alloys SS1 and SS2, strength and hardness are high and ductility is relatively unaffected by the interstitial nitrogen. Upon aging these alloys, both Cr_2N and CrN precipitates nucleate, reducing ductility and impact toughness. The wear rate is unaffected when small abrasive particles are used (e.g., 20 μm SiC). However, when the abrasive particle size becomes large (e.g., 150-grit garnet), wear resistance decreases due to the decrease in ductility and impact fracture toughness. For alloys with substantially more nitrogen than can be accommodated interstitially, coarse CrN precipitates form. These precipitates significantly influence the abrasive wear characteristics of the alloy, particularly when they are large (i.e., 50 μm in width). It is anticipated that modifications to the basic steel composition that incorporates a "harder" nitride (e.g., niobium or vanadium) will lead to superior wear behavior.

Acknowledgments

The authors would like to thank Mr. Neal Duttlinger for metallographic sample preparation and optical microscopy, and Mr. Dale Govier for x-ray diffraction analyses.

References

1. R.P. Reed, *J. Met.*, March 1989, p 16
2. M.O. Speidel and R.M. Pedrazzoli, High Nitrogen Stainless Steels in Chloride Solutions, *Mater. Perform.*, Vol 31(No. 9), 1992, p 59
3. R.D. Pehlke and J.F. Elliott, Solubility of Nitrogen in Liquid Iron Alloys. 1. Thermodynamics, *Trans. AIME*, Vol 218, Dec 1960, p 1088
4. A.H. Satir-Kolorz and H.K. Feichtinger, On the Solubility of Nitrogen in Liquid Iron and Steel Alloys Using Elevated Pressure, *Z. Metallkd.*, Vol 82(No. 9), 1991, p 689

5. J.C. Rawers, N.A. Gokcen, and R.D. Pehlke, High Nitrogen Concentration in Fe-Cr-Ni Alloys, *Metall. Trans. A*, Vol 24A, Jan 1993, p 73
6. K.J. Irvine, D.T. Llewellyn, and F.B. Pickering, High-Strength Austenitic Stainless Steels, *J. Iron Steel Inst.*, Vol 199, 1961, p 153
7. G. Stein, J. Menzel, and H. Dorr, Industrial Manufacture of Massively Nitrogen-Alloyed Steels, *Proc. Int. Conf. on High Nitrogen Steels*, J. Foct and A. Hendry, Ed., Institute of Metals, London, 1989, p 32
8. M.L.G. Byrnes, M. Grujicic, and W.S. Owen, Nitrogen Strengthening of a Stable Austenitic Stainless Steel, *Acta Metall.*, Vol 35(No. 7), 1987, p 1853
9. M. Harsenmoser et al., The Influence of Nickel and Nitrogen on the Mechanical Properties of High-Nitrogen Austenitic Steels at Cryogenic Temperatures, *Proc. 2nd Int. Conf. on High Nitrogen Steels*, G. Stein and H. Witulski, Ed., Verlag Stahleisen, Dusseldorf, 1990, p 197
10. G. Stein, J. Menzel, and M. Wagner, N-Alloyed Steels for Retaining Rings and Other Applications, *Proc. 2nd Int. Conf. on High Nitrogen Steels*, G. Stein and H. Witulski, Ed., Verlag Stahleisen, Dusseldorf, 1990, p 399
11. A. Nyilas and B. Obst, Tensile and Fracture Properties of High Nitrogen Bearing Austenitic Steels at Cryogenic Temperatures, *Proc. Int. Conf. on High Nitrogen Steels*, J. Foct and A. Hendry, Ed., Institute of Metals, London, 1989, p 194
12. R. Ebner, M. Panzenbock, and H. Aigner, Metallurgical Factors Affecting the Fatigue Properties of High Strength Cr-Mn-N Steels, *Proc. 2nd Int. Conf on High Nitrogen Steels*, G. Stein and H. Witulski, Ed., Verlag Stahleisen, Dusseldorf, 1990, p 177
13. *Metals Handbook*, 9th ed., Vol 3, *Properties and Selection: Stainless Steels, Tool Materials, and Special-Purpose Metals*, ASM International, 1980, p 19-23
14. J.W. Simmons, J.C. Rawers, and D.G. Atteridge, Low-Ductility Room Temperature Impact Fracture of High-Nitrogen Austenitic Stainless Steels Induced by Transgranular and Grain Boundary Nitrides, *Microstructural Science*, Vol 21, International Metallographic Society and ASM International, 1992
15. H. Chandra Holm, P.J. Uggowitzer, and M.O. Speidel, Influence of Annealing Temperature on the Microstructure and Mechanical Properties of a High Nitrogen Containing Austenitic Stainless Steel, *Scr. Metall.*, Vol 21, 1987, p 513
16. J. Menzel, G. Stein, and P. Dahlmann, Manufacture of N-Alloyed Steels in a 20t PESR Furnace, *Proc. 2nd Int. Conf on High Nitrogen Steels*, G. Stein and H. Witulski, Ed., Verlag Stahleisen, Dusseldorf, 1990, p 365
17. R. Blickensderfer and G. Laird II, A Pin-on-Drum Abrasive Wear Test and Comparison with Other Pin Tests, *J. Test. Eval.*, Vol 16, 1988, p 516
18. M. Kikuchi, M. Kajihara, and S. Choi, Cellular Precipitation Involving Both Substitutional and Interstitial Solutes: Cellular Precipitation of Cr_2N in Cr-Ni Austenitic Steels, *Mater. Sci. Eng.*, Vol A146, 1991, p 131